Batch mixing study of granular materials in an innovative mixer: the Triaxe®.

Demeyre Jean-François[a], Gatumel Cendrine[a], Berthiaux Henri[a], Grandjean Michel[b]

[a]Chemical Engineering Laboratory for Particulate Solids, UMR CNRS 2392,
Ecole des Mines d'Albi-Carmaux, Campus Jarlard, 81013 Albi Cedex 09 (France)
[b]Hognon SA, rue Antoine Laurent de Lavoisier, 77720 Mormant (France)

Abstract
The object of this work is to characterize the operation of mixing in a new powder mixer, the Triaxe® for which systems with free flowing and cohesive media are studied. We show that this mixer, that combines two motions of agitation, is a very low energy consumer one, in particular for cohesive powders. The influence of the combination of gyrational and rotational speeds is particularly studied. The results are expressed in terms of effective torque and power consumption.
Key-words
Mixing, Granular Systems, Dimensionless number, Power Consumption.

Introduction

In the every day life we are consuming blended solid products as cosmetics, pharmaceuticals and food but also cements, plastics, chemical specialities... The end use properties of these products are more and more complex as they are covering more and more functions. Mixing is the main operation which permits to formulate these products, and therefore guarantees their properties.

Particulate systems are classified according to several properties that may be defined at various scales: size and size distribution, shape and shape distribution, aerated or tapped bulk density, true density, flowing indices... Two main categories of particulate systems are distinguished:

Free flowing powders: these powders are flowing very easily and do not pose any problem of mottage. Each particle has a strong individual mobility, that may correspond to a strong tendency to segregate within a mixture.

Cohesive powders: these powders have strong interparticle strength such as van der Waals forces or electrostatic forces..., which can involve the formation of agglomerates. For that reason they do not have a real tendency to segregate once the mixture is achieved but the mixing is very hard to achieve because a lot a power is needed to separate the grains to "reorganize" the bulk. In addition the connections may cause flow or storage problems.

The choice of a mixer is therefore conditioned to the type of powders and the type of mixture (composition) at play. Different mixer geometries and agitation devices exist but they are nearly always conceived by empiric methods, as well as they induce a systematic motion which do not allow the achievement of a good mixture at a fine scale (Berthiaux, 2002). For instance, the use of chemical engineering tools, such as correlations between dimensionless numbers, ought to be a considerable contribution.

This work deals with an unconventional batch mixer, the Triaxe®, developed and sale by Hognon S.A. company. Originally built for operating with viscous fluids, this mixer showed its capability to realize good mixtures of granular products. It consists in a spherical tank in which the powder is agitated by the combination of the gyration of the shaft and a classical rotational movement of the helix. Rotation and gyration speeds are independently controlled, allowing numerous combinations. This should be able to enhance the mixing process to finally achieve an intimate mixing, at a small spatial scale and probably at the micromixing scale.

Our objective is to quantify the effectiveness of this mixer with different granular systems in terms of homogeneity of the mixtures and characterization of agitation. In this work, we focus on this last aspect by studying the power consumed by this mixer, according to the various operating conditions: combination of velocities and type of powder. Thanks to the measurements of the torque developed by each engine (gyration and rotation) we seek to establish correlations between numbers without dimension as the Froude and Newton numbers, in order to emphasize different mixing modes.

1 Materials and methods

1.1 Particulate systems involved

The solids used are: free flowing powders (couscous and semolina) as well as cohesive powders (Lactose GranuLac 140 and Talc).

1.1.1 Bulk properties

The true densities of the semolina and the couscous were measured with the Helium pycnometer (Accumulator Pyc 1330, Micromeritics). The packed densities were measured by a volumenometer. In this one, a known powder mass is introduced into a graduated test-tube of 250 cm^3 and the bulk volume is recorded after a certain number of shocks (500 taps). We can note that the densities of the free flowing powders are very close (cf. table 1). From these values, we can determine the Carr index (flowability) and Hausner ratio (compressibility).

$$\text{Carr index} = 100 \times \frac{\rho_{\text{packed}} - \rho_{\text{aerated}}}{\rho_{\text{packed}}} \tag{1}$$

$$\text{Hausner ratio} = \frac{\rho_{\text{packed}}}{\rho_{\text{aerated}}} \tag{2}$$

Table 1: Various densities and indices of the products – $^{+}$established with the Helium pycnometer – *established with a volumenometer

Density [$kg{\cdot}m^{-3}$]	Talc	Granulac 140	Semolina	Couscous
True^{+}	2.81	1.54	1.45	1.43
Aerated*	0.509	0.63	0.76	0.72
Packed* (500 taps)	1.083	0.90	0.82	0.76
Carr index	53 %	30 %	7.3 %	5.3 %
Hausner ratio	2.13	1.43	1.08	1.06

The cohesive systems show their differences by initially occupying a more important volume which does not resist to tapping (cf. table 1). In any case, the values of the aerated densities are used as a point of comparison between the powders as the bulk inside a mixer should be aerated for a good mixture achievement.

1.1.2 Particle size distribution

The particle size distributions of couscous and semolina were measured by sieving with control of the amplitude and the duration on a standardized series of sieve. For lactose, it has been obtained by laser diffraction using a dry mode Malvern Mastersizer instrument. The results are given in table 2.

Table 2: characteristic particle diameters of semolina and couscous – $^{+}$established with the laser particle-measurement instrument – *established by sifting

Diameter [µm]	Talc^{+}	Granulac 140^{+}	Semolina*	Couscous*
d_{10}	3.3	20	200	1100
d_{50}	12.6	70	340	1400
d_{90}	33.3	140	840	1800
$Span = \frac{d_{90}-d_{10}}{d_{50}}$	2.37	1.71	1.88	0.5

1.2 Mixer equipment

1.2.1 The Triaxe®

The Triaxe® is a mixer made up of a spherical tank (cf. figure 1) and composed of two engines for the agitation of the mixtures:

- The lower engine involves the axis of gyration, for axis speeds ranging from 0 to 30 rpm. This vertical axis is centered in the tank. Gyration can be carried out clockwise and anti-clockwise direction.
- The higher engine involves the rotation of the agitation device, for axis speeds ranging from 0 to 100 rpm. The blades of the mobile describe a disc around the axis of rotation. Note that this axis is tilted of 15° compared to the horizontal.

Each blade tilting compared to the plan described by the blades axes what introduces a third axis. The combination of stirring velocities and the slope of the blades must make it possible to vary the conditions of flow in order to obtain a satisfying mixture. Moreover, there are various types of blades: full, openwork (used in this study) or out of knives in order to adapt to different powder flow problems.

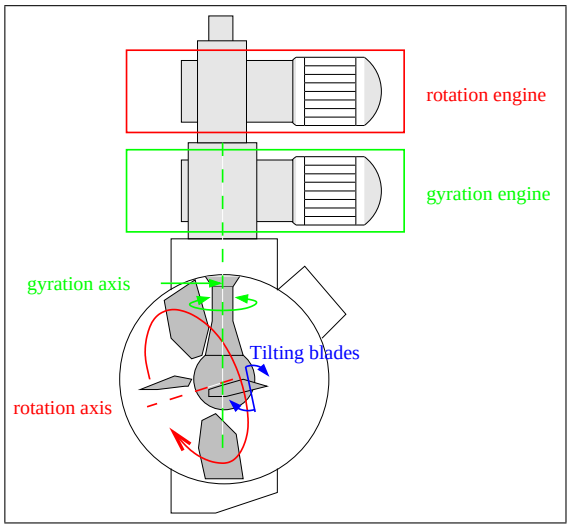

Figure 1: Sketch of the Triaxe®

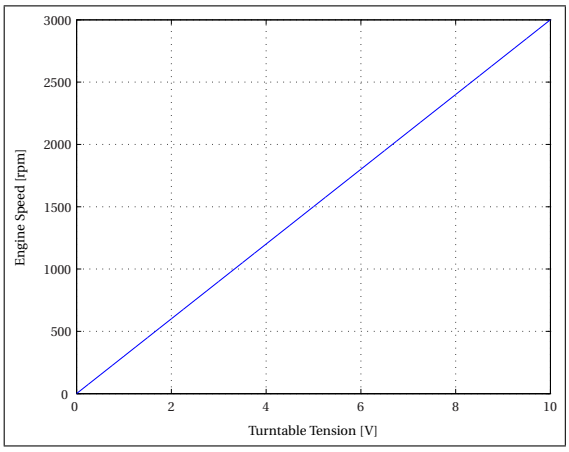

Figure 2: Calibration curve for the speeds of the engines

The two engines Sew Usocome have a power of 370 Watt. Each engine is controlled by a Movitrac turntable. This turntable varies the frequency of the engine supply according to the tension which is applied, between 0 and 10 V. By measuring this tension, we determine the number of revolutions of the engines between 0 to 3000 rpm (cf. figure 2).

Knowing the reduction ratios at the exit of the engines, we deduce N_{A_G} the speed of revolution from the axes of gyration and N_{A_R} the speed the axis of rotation (cf. equation 3)

$$N_{A_G} = \frac{N_{E_G}}{144.79} \quad \text{and} \quad N_{A_R} = \frac{N_{E_R}}{34} + 0.59 N_{A_G} \tag{3}$$

Where N_{E_G} and N_{E_R} are respectively the speed of the engine of gyration and rotation.

1.2.2 Measure of power consumption

Between each engine and the corresponding reducer, a rotary torquemeter of the society Scaime measuring the torque from 0 to 5 N·m has been placed. This allowed to know the power consumption of the two engines. The acquisition of these signals (voltage of each turntable, torque developed by each engine) has been carried out thanks to a National Instruments card PCI-6023E. The data were collected thanks to the software LabVIEW 7.1, and then analyzed by the software Matlab.

The torque developed by each engine has been measured at the following engine speeds: 0, 75, 150, 225, 300, 450, 600, 900, 1200, 1800, 2400, and 3000 rpm. Also, we recorded points of measurements every

100 milliseconds on an interval of one minute to achieve the stability of the signal. The value of the torque used is the average of the acquired data. In order to obtain the value of the torque received by the agitated product, we carried out no-load tests. This allowed us to get free from the mechanical losses:

$$T = T_{\text{in load}} - T_{\text{no load}} \tag{4}$$

The total useful torque is the sum of the useful torque measured on each axes. In the same way, the power consumption P_C is the sum of the useful output of gyration P_G and of rotation P_R:

$$P_C = P_G + P_R \tag{5}$$

With $P_G = (T_G - T_{G_0}) \cdot 2\pi \cdot N_{E_G}$ and $P_R = (T_R - T_{R_0}) \cdot 2\pi \cdot N_{E_R}$. N_{E_G} and N_{E_R} are the speeds of the engines in round·sec^{-1}. Indeed, the torque is measured at exit of the engines and not on the gyration and rotation axes.

1.2.3 Trajectory and speed

We calculate the coordinates of the blades (cf. appendix A) versus time and speed. A trajectory of two of the four blades is presented figure 3.

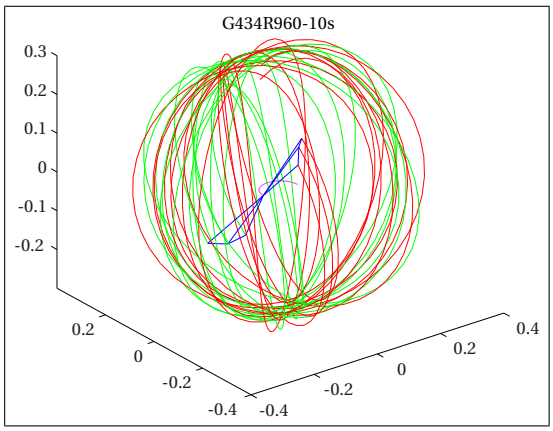

Figure 3: trajectory of two of the four blades of the Triaxe® for engine speed of $N_{E_G} = 434$ rpm and $N_{E_R} = 960$ rpm. after 10 s of mixing

Knowing the trajectory we calculated the linear tip speed of the blade. An example of this speed is shown figure 4.

With the linear tip speed, we defined the penetration angle by the equation (6).

$$\theta = \arctan\left(\frac{\left\|\vec{v}_{n(\vec{x},\vec{y},\vec{z})}\right\|}{\left\|\vec{v}_{t(\vec{x},\vec{y},\vec{z})}\right\|}\right) \tag{6}$$

An example of the evolution of this angle is shown figure 5.

For each couple of engine speed (N_{E_G}, N_{E_R}), the linear tip speed and the angle of penetration strongly vary. We decided to take the maximum of those values in the following developments because they seem to be representative of the influence of the ratio N_{A_R}/N_{A_G}.

2 Results and discussions

2.1 Torque and power consumption

Figure 6 gives the results of the measurements of the useful torque obtained on the two axes for tests on Couscous, Semolina, Lactose and Talc. We always mix 48 l of products, which represent 34.5 kg of couscous,

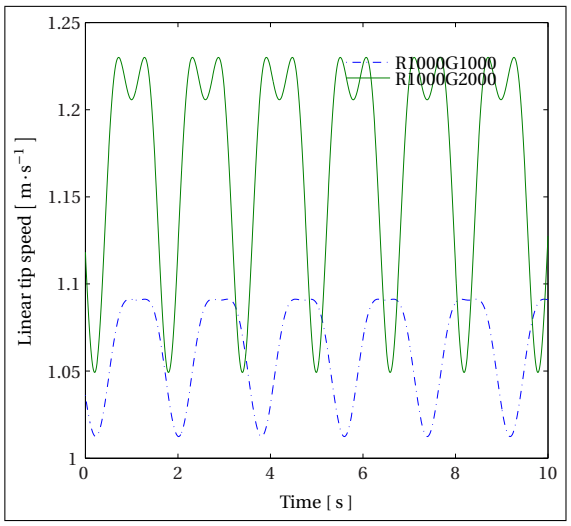

Figure 4: Example of linear tip speed for couples of engine speed (N_{E_G},N_{E_R}) of (1000,1000) and (1000,2000) [rpm]

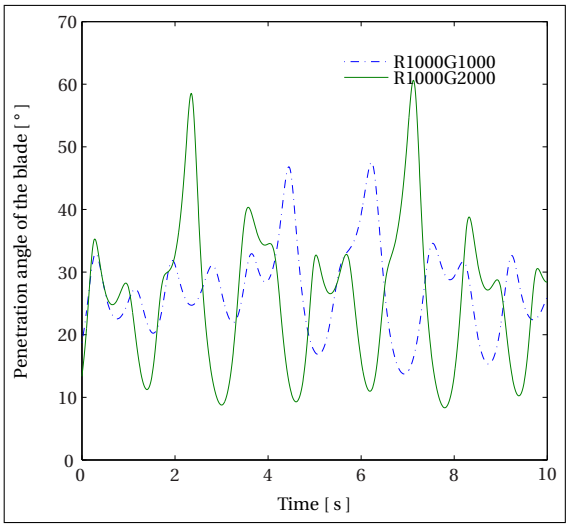

Figure 5: Penetration angle of the blade into the product for couples of engine speed (N_{E_G},N_{E_R}) of (1000,1000) and (1000,2000) [rpm]

36.5 kg of semolina, 30 kg of lactose and 24.5 kg of talc. Each graphics of figure 6 describes, for a couple Product/Engine, the useful torque developed by the engine according to its speed for various speeds of the other engine. For example, figure 6(a) describes the useful torque developed by the engine of gyration for a test on Couscous. The various series of figure 6(a) correspond to various speeds of the engine of rotation.

The useful torque is mainly brought by the rotational movement. For same values of the engine speed, the useful torque brought by the engine of rotation is approximately 3 times more important than the one brought by the engine of gyration.

The torque developed by the engine of gyration depends on the speed of the engine of rotation. The higher the speed of the engine of rotation, the lower the torque brought by the engine of gyration. It may be argued that the torque brought by the engine of rotation facilitates the displacement of the axes of gyration within the product. On the other hand, for each speed of the engine of gyration, the torque developed by the engine of rotation is appreciably the same one.

In rotation or gyration, we always observe a phase of growth of torque with speed, and a plateau phase where the torque is independent of the speed of the engines. The phase of growth lets think that it acts of a viscous mode. Knight et al. (2001) found the factors that determine the impeller torque of vertical axis high speed mixers containing granular solids of low cohesion (sand). When a plate is observed, Knight et al. (2001) showed that the powder rotated as a rigid body in a mode of friction. However, we notice visually that in the Triaxe®, the powders seem to be fluidized and not moved of only one rigid body. This fluidized mode could explain that the torque do not increase any more with the rotational speed.

For the cohesive powder, there exist a maximum between these two phases, corresponding to a “critical speed”. Once the lactose is in motion, it seems to be slightly fluidized, which decreases the interparticle cohesion forces. The torque required is therefore less important. This could explain why the measured torque decreases after the “critical engine speed”. The maximum torque developed for the cohesive powder is more important than for the free flowing powders.

Figure 7 shows that the power consumption for the cohesive powders is lower than that consumed for couscous or semolina. Moreover, it is interesting to note that the mixer never consumed more than 540 W on couscous, 483 W on semolina, 171 W on lactose and 64 W on talc. We can estimate the specific power to be of the order of 15.6 W·kg^{-1} for couscous, 13.2 W·kg^{-1} for semolina and 5 W·kg^{-1} for lactose.

2.2 Dimensionless approach

Empirical correlations between dimensionless numbers (generally the Power number, Np and the Froude number, Fr), in which bulk powder flow characteristics in the mixer under consideration are included through constants, have always been used in the literature. To argue this, one may refer to the general paper by Miyanami (1991) the correlations of Sato & al. for a horizontal drum mixer in Sato et al. (1977) or

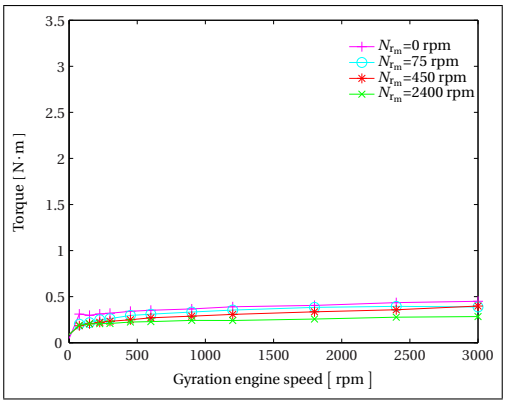

(a) Couscous/Gyration

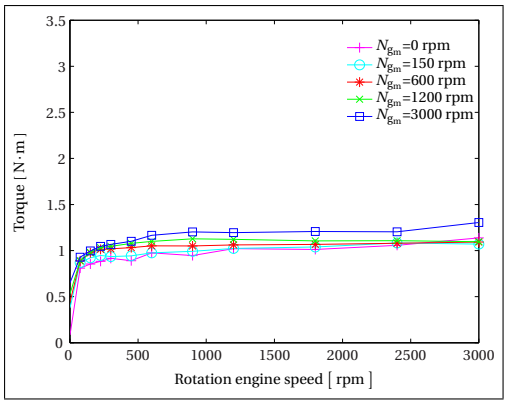

(b) Couscous/Rotation

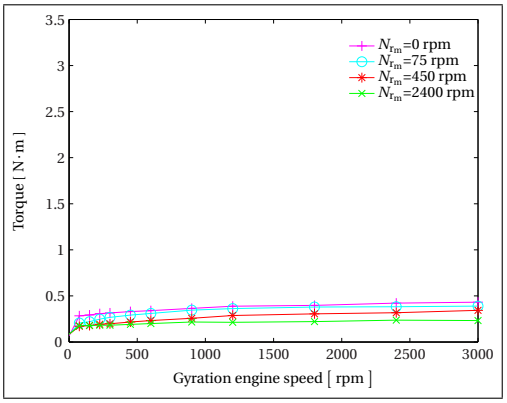

(c) Semolina/Gyration

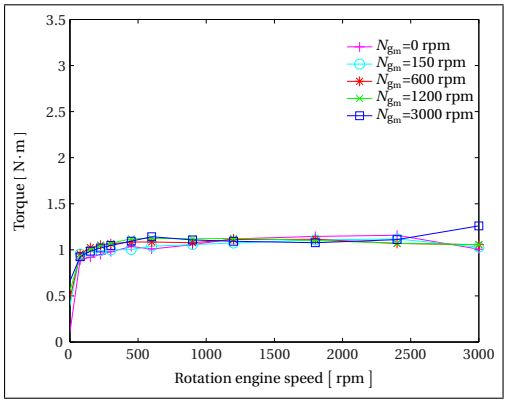

(d) Semolina/Rotation

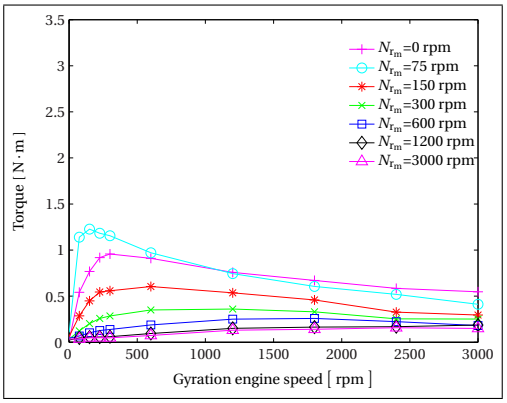

(e) Lactose/Gyration

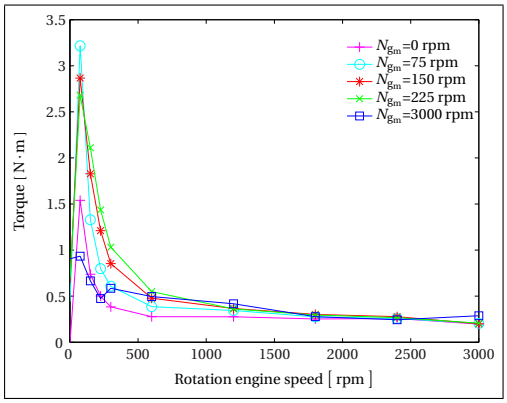

(f) Lactose/Rotation

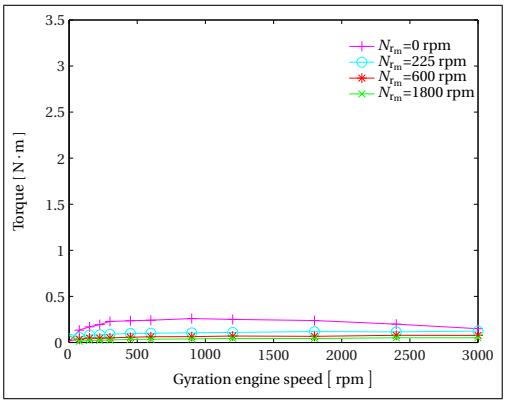

(g) Talc/Gyration

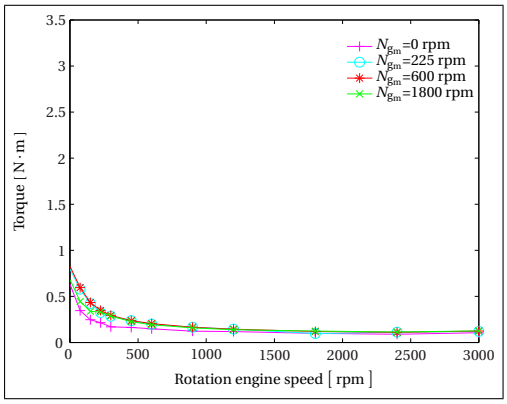

(h) Talc/Rotation

Figure 6: Torque measured on a driving shaft according to its speed. Each series corresponds to a speed of the other engine. Each graph corresponds to a couple product/engine

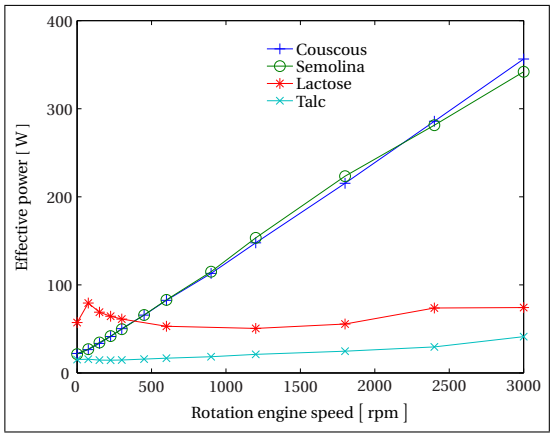

Figure 7: Comparison of the effective power for the 4 products vs. rotation engine speed with N_{E_G} = 600 rpm

a ribbon mixer in Sato et al. (1979), the relations of Entrop (1978) for a screw mixer, of Werther (1976) for a fluidized bed. This is very useful to compare different mixing systems, to avoid the influence of a parameter (size of mixer, mass of product), to show the transition between different flow modes...

We could not represent Np vs. Re because, conversely to the case of fluids, we are not enable to define properly the viscosity of the system. And if we use the torque in place of the viscosity, the representation Np_m vs. Re_m has no sense because the torque is used in the power term of Np_m and in the Re_m (cf. equation (7)).

$$Re_m = \frac{D_{\text{blade}}^3 \cdot v_{\text{max}}^2 \cdot \rho}{T} \text{ and } Np_m = \frac{P}{\rho \cdot v_{\text{max}}^3 \cdot D_{\text{blade}}^2} \tag{7}$$

So, We chose to represent the Newton number Ne as a function of the Froude number Fr_{max}. Fr_{max} is a Number of Froude calculated with characteristic dimensions of the Triaxe®. The number of Newton Ne is a dimensionless Torque, which is interesting because we can compare different experiments with different masses of products.

With the maximum of the linear tip speed v_{max}, we defined

$$Ne = \frac{T}{M \cdot g \cdot L_{\text{blade}}} \text{ and } Fr_{\text{max}} = \frac{v_{\text{max}}}{\sqrt{g \cdot L_{\text{blade}}}} . \tag{8}$$

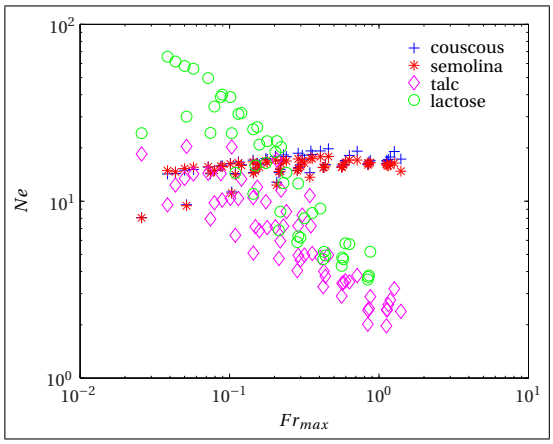

Figure 8: Ne vs Fr_{max}

We can see on figure 8 Ne versus Fr_{max} for each product. On the one hand, for the free flowing powders, the data should be well fitted on a curve except for a ratio $N_{A_R}/N_{A_G} = 0.59$. Note that this ratio is not often

used because it correspond to a null rotation speed engine (cf. (3)). On the other and, for the cohesive powders, for one $Fr_{\max}$, there is a big dispersion of Ne. This can be explained by the different penetration angles for a same $Fr_{\max}$. We can see on figure 9 Ne vs $Fr_{\max}$ for cohesive powders and each series correspond to a range of the maximum penetration angles. As the maximum angle of penetration increases, the effective torque also increases (up to 80 degrees).

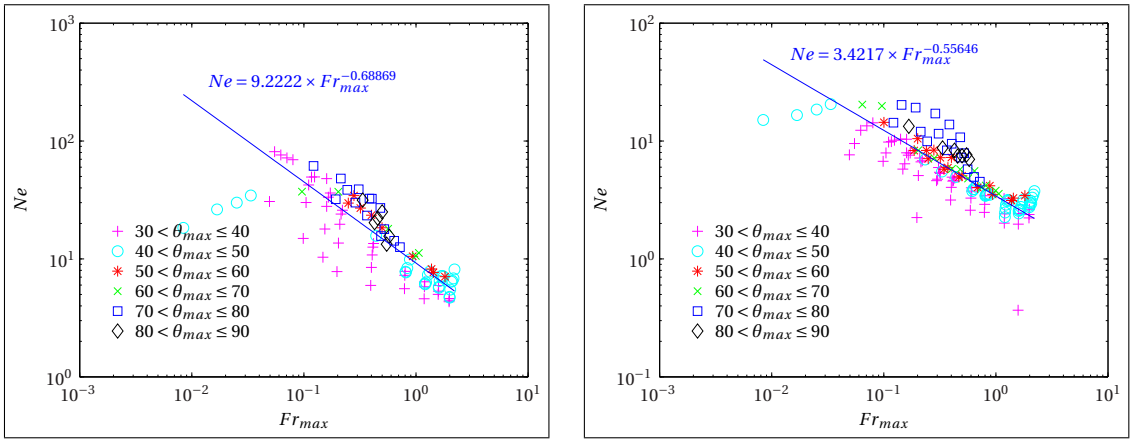

(a) Lactose (b) Talc

Figure 9: Ne vs $Fr_{\max}$ for cohesive powders and different penetration angles

Conclusion

This work is completed on a batch mixer, the Triaxe®, developed and sold by the company Hognon SA. In this work, we are characterizing agitation of particulate systems by studying the power consumed by this mixer according to the various operating conditions: combination of stirring velocities and type of powder. Thanks to measurements of the torque developed by each engine (gyration and rotation) we highlighted the existence of a "critical" speed from which the forces of cohesions are overcome. This speed can be assumed to be a dynamic characterization of the state of cohesion of the system. Furthermore, the differences of torque for a same $Fr_{\max}$ are due to a difference of penetration angle into the product. A short term objective is to connect this work on agitation to a study on the quality of the mixtures in term of homogeneity and of mixing time by an on-line image analysis method.

References

Berthiaux, H. (2002). Mélange et homogénéisation des solides divisés. *Techniques de l'ingénieur*, 397.

Entrop, W. (1978). International symposium on mixing. In Mons, editor, *D1*, pages 1–14.

Knight, P. C., Seville, J. P. K., Wellm, A. B., and Instone, T. (2001). Prediction of impeller torque in high shear powder mixers. *Chemical Engineering Science*, 56(15):4457–4471.

Miyanami, K. (1991). *Mixing Powder Technology Handbook*, pages 595–612. Linoya – Gotoh – Higashitani éditeurs, NY.

Sato, M., Abe, Y., Ishii, K., and Yano, T. (1977). *J. Soc. Powder Technol. Jpn.*, 14:411.

Sato, M., Miyanami, K., and Yano, T. (1979). *J. Soc. Powder Technol. Jpn.*, 16:3.

Werther, W. (1976). *Chem. Eng. Tech.*, 46:339.

Nomenclature

Latin Letters

D_{blade}	the diameter of the blade = $2 \cdot L_{\text{blade}}$	[m]
g	acceleration due to gravity	$[\ \text{m}\cdot\text{s}^{-2}\ ]$
L_{blade}	the legnth of one blade = $\frac{D}{2}$	[m]
M	the mass of product	[kg]
N	speed of revolution	[rpm]
P	Effective power consumption	[W]
T	Torque	[N.m]
$v_{\max}$	the maximum of the linear tip speed	$[\ \text{m}\cdot\text{s}^{-1}\ ]$
v_n	normal speed of the trajectory	$[\ \text{m}\cdot\text{s}^{-1}\ ]$
v_t	tangential speed of the trajectory	$[\ \text{m}\cdot\text{s}^{-1}\ ]$

Greek Letters

ρ	the density of the product	$[\ \text{kg}\cdot\text{m}^{-3}\ ]$

Subscripts

0	idem no load: with no product
A	indicate the axis
E	indicate the engine
G	indicate the gyration
in load	with 48 L of product
no load	with no product
R	indicate the rotation

A Literal expression of trajectory and speed of the Triaxe®

First of all, a sketch of the triaxe (cf. figure 10) to define all the variables needed to calculate the trajectory and speed of the Triaxe®.

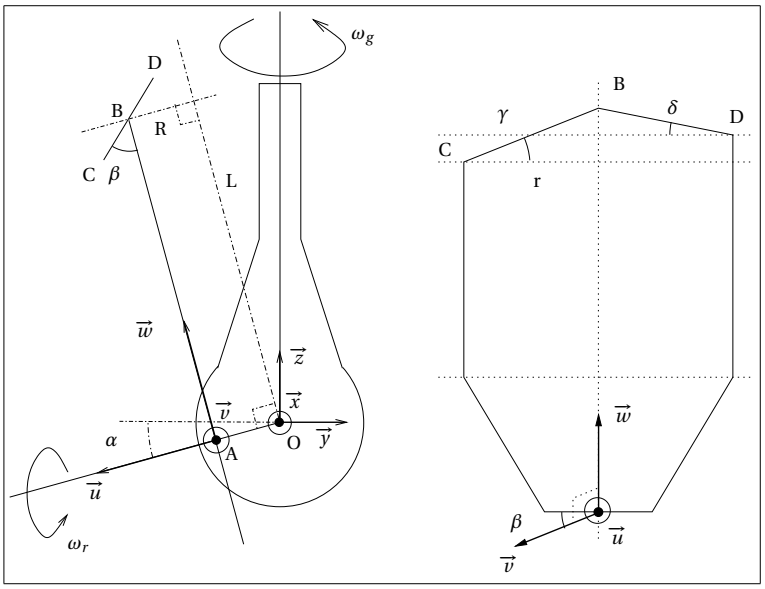

Figure 10: Sketch of the Triaxe®.

We defined the coordinates of $\overrightarrow{u}$, $\overrightarrow{v}$ and $\overrightarrow{w}$ in the laboratory reference frame $(\overrightarrow{x}, \overrightarrow{y}, \overrightarrow{z})$:

$$\overrightarrow{u} \begin{cases} \cos(\alpha)\cos(\omega_g\, t) \\ \cos(\alpha)\sin(\omega_g\, t) \\ -\sin(\alpha) \end{cases} \tag{9}$$

$$\overrightarrow{v} \begin{cases} -\cos(\omega_r\, t)\sin(\omega_g\, t) + \sin(\omega_r\, t)\sin(\alpha)\cos(\omega_g\, t) \\ \cos(\omega_r\, t)\cos(\omega_g\, t) + \sin(\omega_r\, t)\sin(\alpha)\sin(\omega_g\, t) \\ \sin(\omega_r\, t)\cos(\alpha) \end{cases} \tag{10}$$

$$\overrightarrow{w} \begin{cases} \sin(\omega_r\, t)\sin(\omega_g\, t) + \cos(\omega_r\, t)\sin(\alpha)\ cos(\omega_g\, t) \\ -\sin(\omega_r\, t)\cos(\omega_g\, t) + \cos(\omega_r\, t)\sin(\alpha)\sin(\omega_g\, t) \\ \cos(\omega_r\, t)\cos(\alpha) \end{cases} \tag{11}$$

Then,

$$\overrightarrow{OA} = R\,\overrightarrow{u}\ , \tag{12}$$

$$\overrightarrow{AB} = L(\overrightarrow{v} + \overrightarrow{w}) \text{ and} \tag{13}$$

$$\overrightarrow{OB} = \overrightarrow{OA} + \overrightarrow{AB}\ . \tag{14}$$

The coordinates of $\overrightarrow{BC}$ and $\overrightarrow{BD}$ in the rotating reference frame $(\overrightarrow{u}, \overrightarrow{v}, \overrightarrow{w})$:

$$\overrightarrow{BC} \begin{cases} r\sin(\beta) \\ r\cos(\beta) \\ -r\tan(\gamma) \end{cases} \tag{15}$$

$$\overrightarrow{BD} \begin{cases} -r\sin(\beta) \\ -r\cos(\beta) \\ -r\tan(\delta) \end{cases} \tag{16}$$

With

$$\overrightarrow{OC} = \overrightarrow{OA} + \overrightarrow{AB} + \overrightarrow{BC}\ . \tag{17}$$

Considering C to be a point located at an end of the blade, the absolute trajectory of C in the laboratory reference frame is given by the coordinate of $\overrightarrow{OC}$:

$$\overrightarrow{OC} \begin{cases} R\cos(\alpha)\cos(\omega_g\, t) \\ \quad + L\big(-\cos(\omega_r\, t)\sin(\omega_g\, t) + \sin(\omega_r\, t)\sin(\alpha)\cos(\omega_g\, t) \\ \quad + \sin(\omega_r\, t)\sin(\omega_g\, t) + \cos(\omega_r\, t)\sin(\alpha)\cos(\omega_g\, t)\big) \\ \quad + r\sin(\beta)\cos(\alpha)\cos(\omega_g\, t) + r\cos(\beta)\cos(\alpha)\sin(\omega_g\, t) + r\tan(\gamma)\sin(\alpha) \\ R\cos(\alpha)\sin(\omega_g\, t) \\ \quad + L\big(\cos(\omega_r\, t)\cos(\omega_g\, t) + \sin(\omega_r\, t)\sin(\alpha)\sin(\omega_g\, t) \\ \quad - \sin(\omega_r\, t)\cos(\omega_g\, t) + \cos(\omega_r\, t)\sin(\alpha)\sin(\omega_g\, t)\big) \\ \quad + r\sin(\beta)\big(-\cos(\omega_r\, t)\sin(\omega_g\, t) + \sin(\omega_r\, t)\sin(\alpha)\cos(\omega_g\, t)\big) \\ \quad + r\cos(\beta)\big(\cos(\omega_r\, t)\cos(\omega_g\, t) + \sin(\omega_r\, t)\sin(\alpha)\sin(\omega_g\, t)\big) - r\tan(\gamma)\sin(\omega_r\, t)\cos(\alpha) \\ -R\sin(\alpha) \\ \quad + L\big(\sin(\omega_r\, t)\cos(\alpha) + \cos(\omega_r\, t)\cos(\alpha)\big) \\ \quad + r\sin(\beta)\big(\sin(\omega_r\, t)\sin(\omega_g\, t) + \cos(\omega_r\, t)\sin(\alpha)\cos(\omega_g\, t)\big) \\ \quad + r\cos(\beta)\big(-\sin(\omega_r\, t)\cos(\omega_g\, t) + \cos(\omega_r\, t)\sin(\alpha)\sin(\omega_g\, t)\big) - r\tan(\gamma)\cos(\omega_r\, t)\cos(\alpha) \end{cases} \tag{18}$$

Considering B to be a point located at the end of the blade, the absolute velocity of B in the laboratory reference frame is given by the coordinate of $\dot{\overrightarrow{OB}}$:

$$\dot{\overrightarrow{OB}}\begin{cases} -R\cos(\alpha)\sin(\omega_g t)\omega_g + L\big(\sin(\omega_r t)\omega_r \sin(\omega_g t) - \cos(\omega_r t)\cos(\omega_g t)\omega_g \\ \quad + \cos(\omega_r t)\omega_r \sin(\alpha)\cos(\omega_g t) - \sin(\omega_r t)\sin(\alpha)\sin(\omega_g t)\omega_g + \cos(\omega_r t)\omega_r \sin(\omega_g t) \\ \quad + \sin(\omega_r t)\cos(\omega_g t)\omega_g - \sin(\omega_r t)\omega_r \sin(\alpha)\cos(\omega_g t) - \cos(\omega_r t)\sin(\alpha)\sin(\omega_g t)\omega_g\big) \\ R\cos(\alpha)\cos(\omega_g t)\omega_g + L\big(-\sin(\omega_r t)\omega_r \cos(\omega_g t) - \cos(\omega_r t)\sin(\omega_g t)\omega_g \\ \quad + \cos(\omega_r t)\omega_r \sin(\alpha)\sin(\omega_g t) + \sin(\omega_r t)\sin(\alpha)\cos(\omega_g t)\omega_g - \cos(\omega_r t)\omega_r \cos(\omega_g t) \\ \quad + \sin(\omega_r t)\sin(\omega_g t)\omega_g - \sin(\omega_r t)\omega_r \sin(\alpha)\sin(\omega_g t) + \cos(\omega_r t)\sin(\alpha)\cos(\omega_g t)\omega_g\big) \\ L\big(\cos(\omega_r t)\omega_r \cos(\alpha) - \sin(\omega_r t)\omega_r \cos(\alpha)\big) \end{cases} \tag{19}$$